Korean J. of Chem. Eng., **12**(2), 146-151 (1995)

THE EFFECTS OF CAPACITY RATIO ON THE PERFORMANCE OF ALKALINE BATTERIES

Sungmin Hwang, Jaegeon Kim, Sun-Geon Kim and Taewhan Yeu†

Department of Chemical Engineering, Chung-Ang University

(Received 9 December 1993 • accepted 27 October 1994)

Abstract—The effects of cathode/anode capacity ratio on the performance of mercury-free alkaline zinc-manganese dioxide batteries were studied. An alternating current impedance analysis and a continuous discharge test with constant electrical load were employed. The discharge and leakage performances of alkaline batteries varied strongly with capacity ratios and discharge rates. The lower capacity ratios favored discharge performance at high rates, whereas discharge performance at low rates depended only on the quantity of manganese dioxide present. In addition, the lower capacity ratios yielded high in-cell gassing with severe leakage problems, especially at partially discharged cell.

Key words: Alkaline Battery, Cell Capacity, Discharge Performance, Mercury-free

INTRODUCTION

Despite significant advances in the development of new battery systems, an alkaline zinc-manganese dioxide cell is still the most widely used primary battery system in the world [Kordesch, 1984; Vincent, 1984]. This is because of its good shelf life, reasonable energy and power densities (95 Wh/kg and 220 Wh/*l*), good reliability, and cost effectivity. In addition, the alkaline system is continuously replacing the classic Leclanché cell in the market due to its superior reliability and performance at high current drains, continuous discharge, and low temperature. Although the alkaline cell is more expensive than the Leclanché cell due to the use of high quality raw materials and sophisticated construction, it is much more economical in the practical applications [Vincent, 1984; Falk and Salkind, 1992].

Among the various factors which affect alkaline cell performances, the corrosive perforation of the zinc anode is one of the main reasons causing the battery capacity drop, shortening lifetime, and leakage. A simplified overall reaction mechanism for self-discharge can be written as follows [Kordesch, 1984; Vincent, 1984; Falk and Salkind, 1992]:

$$\begin{aligned}&\text{Cathodic Sites}: 2H_2O + 2e^- \rightarrow 2OH^- + H_2\uparrow\\ &\text{Anodic Sites}: Zn + 2OH^- \rightarrow Zn(OH)_2 + 2e\\ &\text{Overall}: Zn + 2H_2O \rightarrow Zn(OH)_2 + H_2\uparrow \end{aligned} \quad (1)$$

Zinc is thermodynamically unstable in contact with alkaline solutions. On storage or rest, the anodic sites of the zinc electrode self-discharges into zinc hydroxide, zinc oxide, or their mixture, with a resulting loss in electrical capacity of the zinc electrode. Simultaneously, the cathodic sites of the zinc electrode generates the hydrogen gas by the decomposition of water. The hydrogen gas generation is particularly undesirable in sealed dry batteries where it can yield excessive pressure build-up with severe leakage problems.

Mercury has been used as a corrosion inhibitor of zinc for a long time. Since mercury has a much smaller exchange current for the hydrogen evolution reaction compared to zinc, amalgamation raises the hydrogen overvoltage and reduces the rate of the corrosion reaction [Delahay, 1965]. Amalgamation also reduces the harmful effects of heavy metal impurities, and improves rate capability by providing better electronic contact between zinc particles and anode current collector.

Since the mid 1980's, battery manufacturers have been under pressure to reduce and finally eliminate mercury from all dry cell batteries due to environmental constraints. The commercial alkaline batteries contained 4 to 8% mercury by weight in the zinc anode, depending on the applications. Two basic approaches taken by battery manufacturers were the use of special zinc alloys [Miura et al., 1988, 1989] and organic corrosion inhibitors [Vignand, 1986; Yamazaki et al., 1989; Larsen and Dopp, 1989]. The mercury content was reduced to as low as 0.025% by most manufacturers by 1991. All of the major producers announced in 1992 the near-term availability of "zero" mercury alkaline cells. However, currently available mercury-free products still show some problems such as high in-cell gassing, shock sensitivity, poor amperage and shelf life, etc.

This study was conducted to minimize these existing problems and improve the discharge performances of mercury-free alkaline zinc-manganese dioxide batteries by understanding the influence of capacity ratio on the discharge and leakage performances of alkaline systems. Capacity ratio is defined here as a theoretical capacity ratio of cathode to anode as follows:

$$\text{Capacity Ratio} = \frac{\text{Theoretical Capacity of Cathode}}{\text{Theoretical Capacity of Anode}} = \frac{0.370\ \text{Ah/g}\times\text{g of Manganese Dioxide}}{0.820\ \text{Ah/g}\times\text{g of Zinc}} \quad (2)$$

Thus, capacity ratio less than one involves excess anode capacity. The values of 0.370 Ah/g and 0.820 Ah/g were used for the theoretical capacities of the manganese dioxide and zinc, respectively.

†All correspondences should be addressed.

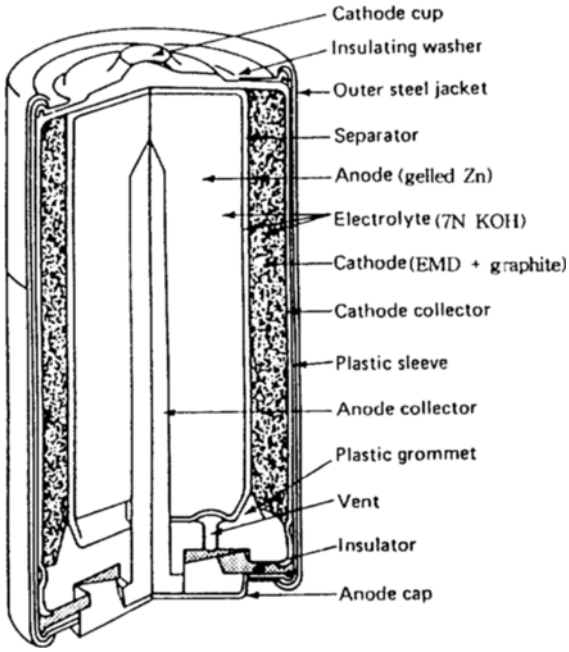

Fig. 1. A schematic diagram of a typical alkaline cell.

Table 1. Targeted cell balance

Capacity ratio	Cathode capacity (Ahr)	Anode capacity (Ahr)
0.975	2.922	2.997
1.000	2.961	2.961
1.025	2.999	2.926
1.050	3.036	2.892
1.075	3.072	2.858

EXPERIMENTS

Mercury-free alkaline cells with various capacity ratios were constructed and tested in this study. AA size was chosen because about 60% of the alkaline cells used are of this size. A schematic diagram of a typical alkaline cell is shown in Fig. 1 [Kordesch, 1984]. The sealed cell consists of a electrolytic manganese dioxide (EMD) cathode on the form of a pellet, a absorbent separator soaked with 7 N KOH solution, and a gelled zinc anode.

The capacity ratios of 0.975, 1.000, 1.025, 1.050, and 1.075 were achieved by altering the weight ratio of cathode powder to gelled anode as shown in Table 1. The cathode volume, void volume, and weight ratio of zinc/electrolyte were maintained constant. Thus, the lower capacity ratio decreases cathode density (with higher porosity) and increases gelled anode height. During the cell construction, great efforts were made to accurately weigh each component in order to achieve the targeted capacity ratio (weight variation of $\pm$ 0.005 g). All materials used in this study were battery grade.

To measure internal resistances, alternating current (AC) impedance analysis was performed five days after the construction [Bard and Faulkner, 1980]. Open circuit voltages (OCV) and impedance data were obtained by using an EG&G Princeton Applied Research (PAR) Model 273A potentiostat/galvanostat and a PAR Model 5210EC two-phase lock-in amplifier interfaced to an IBM compatible 486 personal computer via a National Instrument

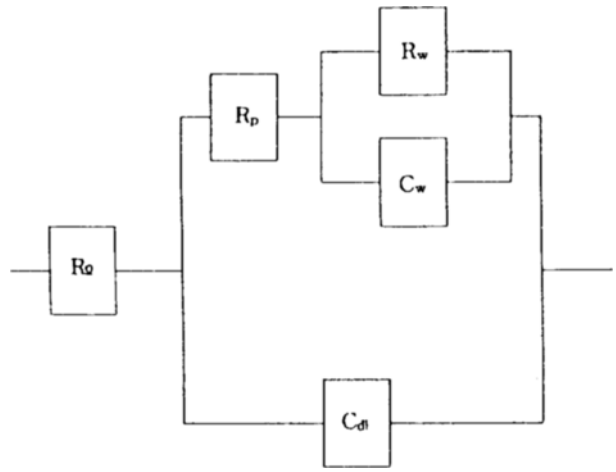

Fig. 2. An equivalent electronic circuit used for an alkaline cell.

Table 2. AC impedance analysis

Capacity ratio	OCV (V)	R_Ω (Ω)	R_p (Ω)
0.975	1.594 [0.004]	0.202 [0.025]	0.324 [0.062]
1.000	1.595 [0.003]	0.135 [0.016]	0.313 [0.027]
1.025	1.594 [0.004]	0.128 [0.006]	0.279 [0.015]
1.050	1.595 [0.003]	0.123 [0.005]	0.266 [0.025]
1.075	1.593 [0.004]	0.120 [0.012]	0.192 [0.008]

Values in [ ] represent standard deviation.
Sample size = 10.

IEEE-488 General Purpose Interface Bus (GPIB). Data were stored and analyzed using PAR M378 software. The applied frequency ranged from 0.2 to 20,000 Hz with an AC voltage signal varying by $\pm$ 10 mV. It was assumed that the alkaline system is equivalent to a simple electronic circuit consisted of uncompensated ohmic resistance (R_Ω), polarization resistance (R_p), double layer capacitance (C_{dl}), and Warburg effects (R_w and C_w) as shown in Fig. 2.

For the discharge performance test, continuous discharge mode with constant electrical loads (R) of 1.0, 2.2, 3.9, 10, 30, and 120 Ω were used to simulate various practical applications such as camera devices, flashes, toys, radios, etc. The cell voltage (E) was recorded as a function of time (t) using a Fluke Model 8050A digital multimeter and a Hewlett Packard Model 7044A X-Y recorder. Throughout the experiments, the room temperature was 25℃. There was no attempt to maintain the temperature of the cells at a constant value during discharge.

For hydrogen gas generation, undischarged and partially discharged cells were stored at 71℃ and monitored for leakage. The partially discharged cells were employed here to simulate realistically a leakage within the electronic devices. 3.9 Ω for 2 hours and 10.0 Ω for 5.5 hours (i.e., approximately 25% of the theoretical capacity of cell) were used. The temperature of 71℃ was used to accelerate the self-discharge. An internal gas volume was then measured for unleaked cells within a sealed container to obtain the dependency of hydrogen evolution by corrosion as a function of capacity ratio.

RESULTS AND DISCUSSION

The results of OCV measurements and AC impedance analysis

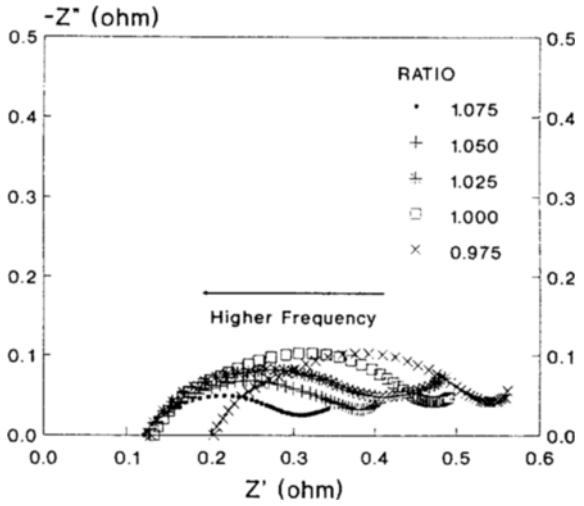

Fig. 3. A Nyquist plane plot for various capacity ratio designs.

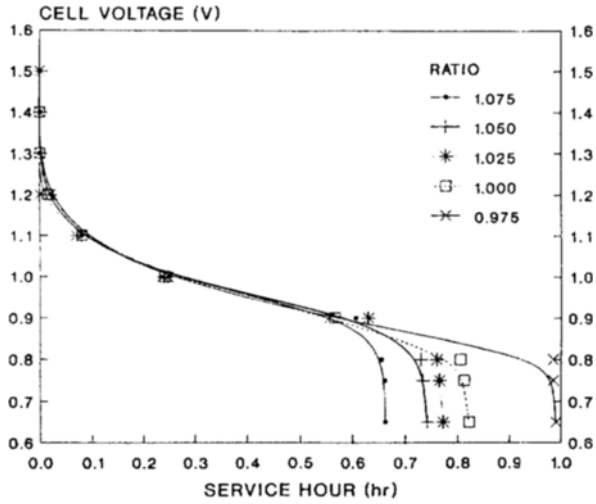

Fig. 4. Continuous discharge performance at 1.0 Ω.

were summarized in Table 2. The values of OCV were not affected by capacity ratio at all. However, both ohmic and polarization impedances (R_Ω and R_p) increased significantly by lowering capacity ratio. The values were expressed as averaged mean values, and the dispersion in the data is given by the standard deviation. A minimum of ten cells were tested.

Fig. 3 shows a complex impedance plane diagram (a Nyquist plane plot) for various capacity ratio designs [Bard and Faulkner, 1980]. While the ohmic resistances (R_Ω) estimated at high frequencies increased from 0.12 to 0.20 Ω with lowering capacity ratio from 1.075 to 0.975, the polarization resistances (R_p) estimated at low frequencies increased from 0.19 to 0.32 Ω. These increases of internal resistance (ohmic and polarization resistances) is thought to be due to loosening of the contact between can and cathode or cathode particles with the less dense cathode composite, and not to capacity ratio.

The cell voltage (E) versus time (t) curves during discharge with various electrical loads (1.0, 2.2, 3.9, 10, 30, and 120 Ω) are presented in Figs. 4 through 9. Discharge curves clearly showed a two-step reduction mechanism of manganese dioxide. The first step is from MnO_2 to MnOOH, producing S-shape curve. Dis-

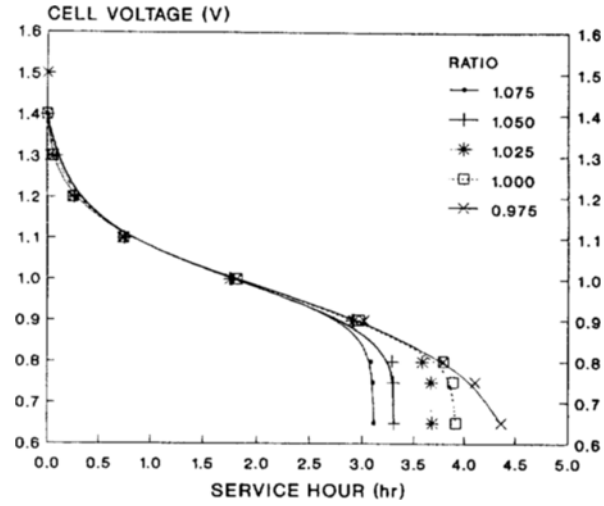

Fig. 5. Continuous discharge performance at 2.2 Ω.

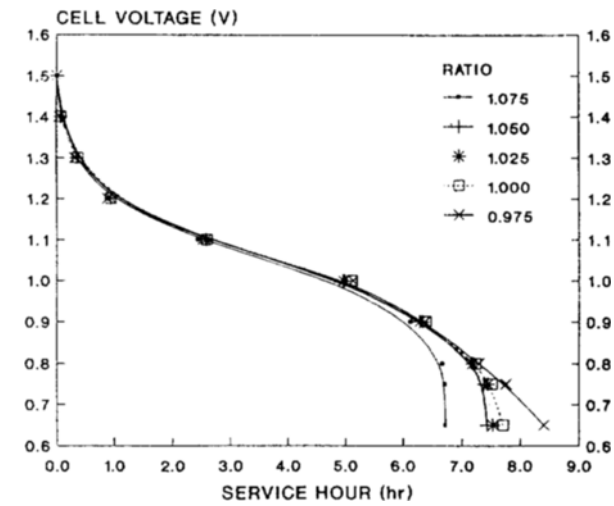

Fig. 6. Continuous discharge performance at 3.9 Ω.

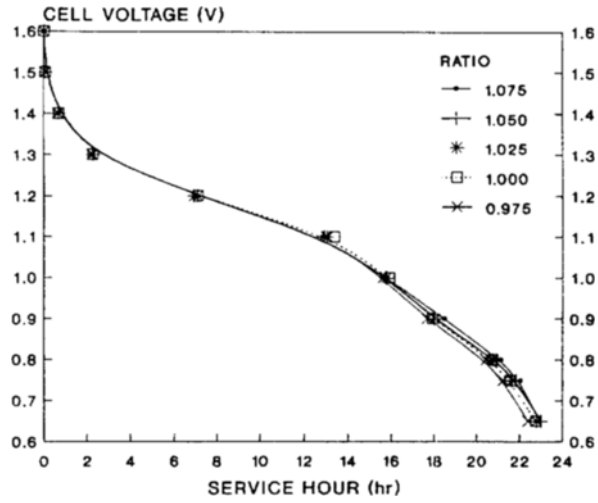

Fig. 7. Continuous discharge performance at 10 Ω.

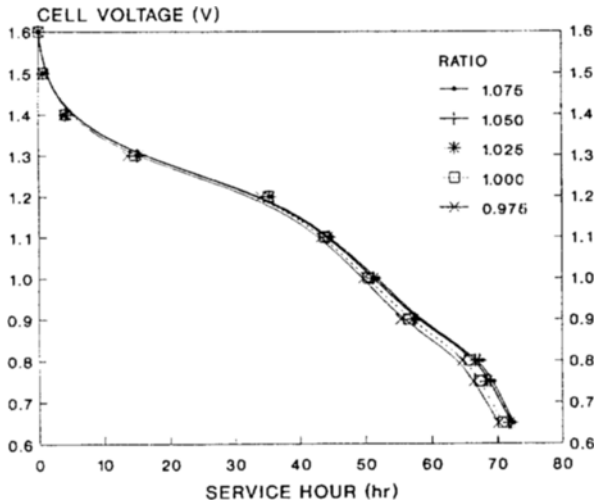

Fig. 8. Continuous discharge performance at 30 Ω.

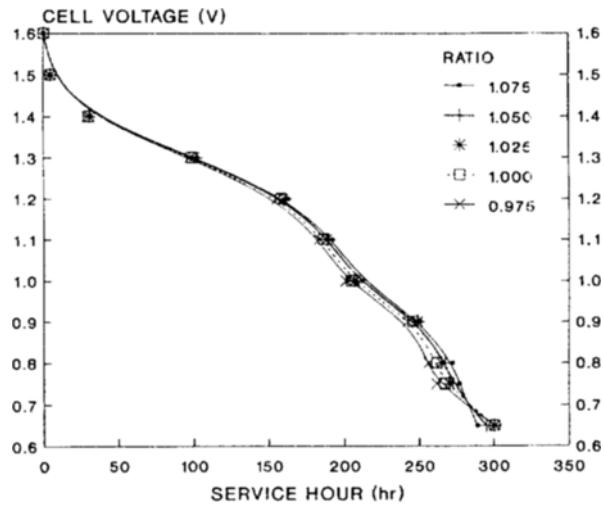

Fig. 9. Continuous discharge performance at 120 Ω.

charges at 1.0, 2.2, and 3.9 Ω showed only this step, whereas those at 10, 30, and 120 Ω showed further reduction from MnOOH to $Mn(OH)_2$.

The discharge performance strongly varied with capacity ratios and discharge rates as expected. At high and moderate discharge rates (1.0, 2.2, 3.9, and 10 Ω), it was interesting that the difference of discharge performance with various capacity ratio were observed at the limited ranges of cell voltage. That is, there is no significant differences in the discharge behavior until the cell voltages reached 0.9 V. The service hours were only extended at the cell voltages lower than 0.9 V with lowering capacity ratio. The differences were more significant at higher discharge rate. At low discharge rates (30 and 120 Ω), on the other hand, there is no significant differences in the discharge behavior regardless of capacity ratios. This is more clearly demonstrated in Table 3, which summarized the service hours at cut-off voltages of 0.9 V and 0.65 V, respectively.

The values of utilized capacity as functions of electrical load and capacity ratio are summarized in Table 4 at cut-off voltages of 0.9 V and 0.65 V, respectively. The utilized capacity was obtained by integrating cell current curve with time as follows [Bard and Faulkner, 1980]:

Table 3. Service hour (hr)

A. At 0.9 V cut-off

Capacity ratio	Discharge load (Ω)					
	1.0	2.2	3.9	10.0	30.0	120.0
0.975	0.56	3.01	6.33	17.6	55.3	242.3
1.000	0.56	2.97	6.38	17.9	56.5	245.8
1.025	0.63	2.91	6.28	18.0	57.2	248.7
1.050	0.63	2.90	6.31	18.0	57.5	249.0
1.075	0.61	2.89	6.01	18.4	57.9	250.5

B. At 0.65 V cut-off

Capacity ratio	Discharge load (Ω)					
	1.0	2.2	3.9	10.0	30.0	120.0
0.975	0.99	4.36	8.26	22.4	70.1	300.6
1.000	0.78	3.92	7.64	22.8	70.8	300.4
1.025	0.76	3.68	7.54	22.8	71.8	300.5
1.050	0.75	3.31	7.44	23.0	72.1	295.0
1.075	0.66	3.13	6.51	23.0	72.4	289.0

Sample size = 10.

Table 4. Utilized capacity (Ahr)

A. At 0.9 V cut-off

Capacity ratio	Discharge load (Ω)					
	1.0	2.2	3.9	10.0	30.0	120.0
0.975	0.551	1.423	1.768	2.061	2.236	2.476
1.000	0.565	1.411	1.788	2.096	2.283	2.513
1.025	0.633	1.383	1.757	2.100	2.314	2.543
1.050	0.627	1.382	1.773	2.100	2.325	2.551
1.075	0.610	1.369	1.683	2.139	2.339	2.569

B. At 0.65 V cut-off

Capacity ratio	Discharge load (Ω)					
	1.0	2.2	3.9	10.0	30.0	120.0
0.975	0.916	1.916	2.157	2.443	2.632	2.837
1.000	0.753	1.770	2.051	2.483	2.668	2.855
1.025	0.745	1.677	2.024	2.481	2.705	2.868
1.050	0.738	1.540	2.008	2.502	2.715	2.845
1.075	0.656	1.460	1.792	2.503	2.731	2.824

Sample size = 10.

$$\text{Utilized Cell Capacity} = \int_0^{t_c} \frac{E}{R}\,dt \tag{3}$$

where R represents the electrical load and t_c represents the time when cell voltage reaches cut-off value. Cell current was obtained from cell voltage by Ohm's law.

It was obvious that the battery system delivered more energy at lower discharge rates. However, the effects of capacity ratio on the utilized capacity varied strongly depending on the discharge rates and cut-off voltages. Thus, anode and cathode efficiencies with various discharge rates and cut-off voltages were calculated as follows:

$$\text{Anode Efficiency} = \frac{\text{Utilized Cell Capacity}}{\text{Theoretical Capacity of Anode}} \tag{4}$$

$$\text{Cathode Efficiency} = \frac{\text{Utilized Cell Capacity}}{\text{Theoretical Capacity of Cathode}} \tag{5}$$

Table 5. Anode and cathode efficiencies (%)

A. Anode efficiency at 0.9 V cut-off

Capacity ratio	Discharge load (Ω)					
	1.0	2.2	3.9	10.0	30.0	120.0
0.975	18.03	46.56	57.84	67.43	73.16	81.01
1.000	18.67	46.62	59.08	69.25	75.43	83.03
1.025	21.13	46.16	58.64	70.08	77.23	84.87
1.050	21.13	46.56	59.74	70.75	78.34	85.95
1.075	20.86	46.82	58.51	73.15	79.99	87.85

B. Cathode efficiency at 0.9 V cut-off

Capacity ratio	Discharge load (Ω)					
	1.0	2.2	3.9	10.0	30.0	120.0
0.975	18.78	48.50	60.26	70.25	76.21	84.39
1.000	19.05	47.17	60.28	70.67	76.97	84.72
1.025	21.12	46.15	58.63	70.07	77.21	84.85
1.050	20.71	45.64	58.56	69.36	76.79	84.25
1.075	19.85	44.54	55.67	69.59	76.10	83.59

C. Anode efficiency at 0.65 V cut-off

Capacity ratio	Discharge load (Ω)					
	1.0	2.2	3.9	10.0	30.0	120.0
0.975	29.97	62.69	70.57	79.93	86.11	92.82
1.000	24.88	58.48	67.77	82.04	88.15	94.33
1.025	24.86	55.97	67.55	82.80	90.27	95.71
1.050	24.87	51.89	67.65	84.30	91.52	95.86
1.075	22.43	49.93	62.90	85.60	93.39	96.57

D. Cathode efficiency at 0.65 V cut-off

Capacity ratio	Discharge load (Ω)					
	1.0	2.2	3.9	10.0	30.0	120.0
0.975	31.22	65.30	73.52	83.27	89.71	96.69
1.000	25.39	59.67	69.15	83.71	89.95	96.25
1.025	24.86	55.96	67.54	82.79	90.26	95.70
1.050	24.37	50.86	66.32	82.63	89.72	93.96
1.075	21.34	47.50	59.84	81.44	88.86	91.88

Sample size = 10.

Table 6. In-cell gas volume after four weeks at 71°C (ml)

Capacity ratio	Undisch.	3.9 Ω & 2 hr	10.0 Ω & 5.5 hr
1.075	0.24 [0.019]	0.73 [0.025]	0.63 [0.028]
1.050	0.24 [0.023]	0.74 [0.045]	0.64 [0.068]
1.025	0.27 [0.024]	0.77 [0.071]	0.66 [0.030]
1.000	0.33 [0.053]	0.93 [0.080]	0.78 [0.032]
0.975	0.42 [0.097]	0.99 [0.097]	0.91 [0.097]

Values in [ ] represent standard deviation.
Sample size = 10.

and summarized in Table 5. At high discharge rates, both the anode and cathode efficiencies were improved with lower capacity ratio. Once again, the efficiency improvements were more significant at the cut-off voltages less than 0.9 V. At low discharge rates, on the other hand, the anode efficiency was impaired with lower capacity ratio regardless of cut-off voltages, while the cathode efficiency was not affected significantly. The anode and cathode efficiencies at the discharge loads of 2.2 and 10 Ω were presented as functions of capacity ratios and cut-off voltages in Figs. 10 and 11, respectively.

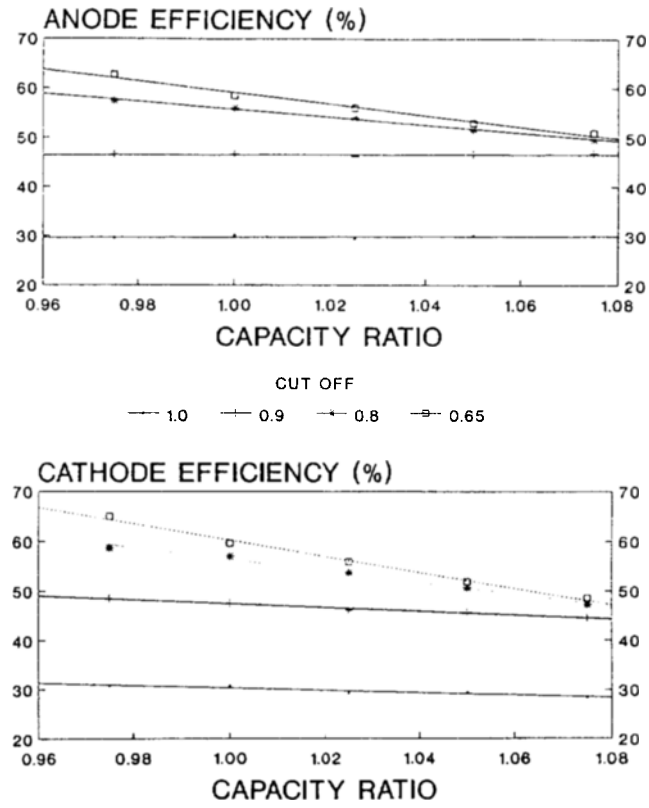

Fig. 10. Anode and cathode efficiencies at 2.2 Ω continuous discharge.

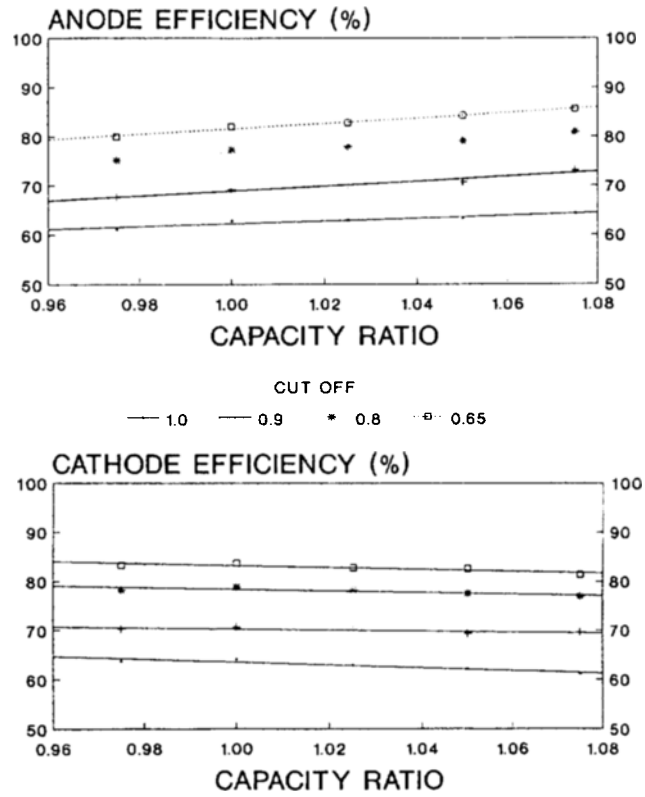

Fig. 11. Anode and cathode efficiencies at 10 Ω continuous discharge.

The results of leakage test are summarized in Table 6. At 71C for four weeks, the lower capacity ratio yielded higher in-cell gas volume with more leakage. This is because more zinc and electrolyte are available for self-discharge (hydrogen evolution) with lower capacity ratio. In addition, partially discharged cell produced much more hydrogen gas compared to undischarged cell. Also, the higher discharge rate (3.9 Ω for 2 hours compared to 10.0 Ω for 5.5 hours) produces more hydrogen gases. That is, the leakage potential was increased within the electronic devices compared to the supermarket stands, and camera flashes compared to smoke detector.

CONCLUSIONS AND RECOMMENDATIONS

The results showed that the discharge performance improved at high discharge rates with lower capacity ratio. However, the higher in-cell gassing with lower cell capacity ratio resulted in more gas production and leakage. It should be noted that there is no benefit of lowering capacity ratio at low discharge rates. These observations make to conclude that the capacity ratio of 1.025 can be the low limit for safety.

In this study, several simplifications were used such as, constant electrolyte/zinc ratios, constant void volumes, etc. With different material types (zinc, manganese dioxide, graphite, etc.) or cell designs, further analysis will be necessary. In addition, continuous discharge mode with constant resistances was employed in this study. For practical applications, batteries can be discharged under a constant load, a constant current, a constant power, or various pulsing modes. The results may be slightly different depending on discharge modes.

NOMENCLATURE

C_{dl} : double layer capacitance [F]
C_w : Warburg capacitance [F]
E : cell voltage [V]
R : electrical load [Ω]
R_p : polarization resistance [Ω]
R_w : Warburg resistance [Ω]
R_Ω : ohmic resistance [Ω]
t : time [hr]
t_c : time when cell voltage reaches cut-off value [hr]
Z′ : real component of impedance [Ω]
Z″ : imaginary component of impedance [Ω]

REFERENCES

Bard, A. J. and Faulkner, L. R., "Electrochemical Methods-Fundamentals and Applications", John Wiley & Sons, New York, 1980.
Delahay, P., "Double Layer and Electrode Kinetics", Interscience, New York, 1965.
Falk, S. U. and Salkind, A. J., "Alkaline Storage Batteries", John Wiley & Sons, New York, 1992.
Kordesch, K. V., "Handbook of Batteries & Fuel Cells", McGraw-Hill, New York, 1984.
Larsen, D. M. and Dopp, R. B., US Patent 4857424, 1989.
Miura, A., Okazaki, R., Takata, K. and Ohira, T., US Patent 47 35876, 1988.
Miura, A., Takata, K., Okazaki, R., Uemura, T. and Kagawa, K., US Patent 4861688, 1989.
Vignaud, R., US Patent 4606984, 1986.
Vincent, C. A., "Modern Batteries, An Introduction to Electrochemical Power Sources", Edward Arnold, London, 1984.
Yamazaki, S., Abe, M., Nagayama, S., Suzuki, K., Fukada, T., Kinka, M., Shibata, K. and Susukida, M., US Patent 4847669, 1989.